A 3-D Polarized Reversed Monte Carlo Radiative Transfer Model for Millimeter and Submillimeter Passive Remote Sensing in Cloudy Atmospheres

Cory Davis, Claudia Emde, and Robert Harwood

Abstract—This paper introduces a three-dimensional (3-D) polarized radiative transfer model that has been developed to assess the influence of cirrus clouds on radiances measured by the Earth Observing System Microwave Limb Sounder (EOS-MLS) instrument. EOS-MLS is on the Aura satellite, which launched in July 2004. The radiative transfer model uses a reversed Monte Carlo algorithm and has been incorporated in the Atmospheric Radiative Transfer Simulator 1.1.x software package. The model will be used to study aspects of the scattering problem that are not considered in the existing operational EOS-MLS cloudy-sky forward model, including the influence of nonspherical, oriented hydrometeors, and 3-D inhomogeneous cloud structure. This paper presents the radiative transfer algorithm and example model results, which demonstrate significant 3-D and polarization effects. Although the development of this model was motivated by the EOS-MLS mission, it is also directly applicable to ground-based and down-looking geometries.

Index Terms—Clouds, polarization, radiative transfer, remote sensing, scattering.

I. INTRODUCTION

MICROWAVE limb sounding (MLS) is a powerful technique for obtaining high vertical resolution measurements of trace gases in the stratosphere and upper troposphere. The microwave region has an advantage over shorter wavelengths because measurements are less affected by liquid water clouds. However, cirrus clouds, with particle sizes often exceeding microwave wavelengths, can severely disrupt trace gas measurements. On the other hand, it is possible to obtain cloud information from MLS radiances affected by cirrus clouds. The first requirement in defining the conditions where trace gas and cloud measurements are possible is a radiative transfer model that can simulate the scattering of atmospheric thermal radiation by cirrus clouds.

The nonsphericity of cirrus particles complicates the modeling task. Cirrus clouds also have finite spatial extent and internal structure. In order to account for these possibly significant features, this study treats the problem as rigorously as possible by considering nonspherical cirrus particles and polarized three-dimensional (3-D) radiative transfer. In the past (e.g., [1]), and particularly in operational retrieval software [2], excessive

C. Davis and R. Harwood are with the School of Geosciences, University of Edinburgh, Edinburgh EH9 3JZ, U.K. (e-mail: cory@met.ed.ac.uk).

C. Emde is with the University of Bremen, 28359 Bremen, Germany.

CPU demands have necessitated the approximations of equivalent spherical particles, and one-dimensional (1-D) radiative transfer in scattering calculations.

A survey of existing freely available radiative transfer models yielded none that were well suited to the MLS problem. For instance, SHDOM [3] is unpolarized, requires particles to be spherical, and its Cartesian geometry is not well-suited to the limb sounding problem. Forward Monte Carlo radiative transfer (RT) models, such as the freely available GRIMALDI [4], can be impractical for radiance measurement remote sensing applications because of the prohibitively large number of photons required to give meaningful results for a narrow field of view.

Discrete ordinates (DOM) type methods are attractive when simulating the whole radiation field, but in the limb sounding— and other remote sensing cases—only a very limited subset of outward propagation paths are required. Also, for limb sounding simulations there is a strong variation in incoming radiance with zenith angles close to 90°. In DOM type models, this necessitates a very fine angular grid, which can be expensive.

A reversed Monte Carlo method was chosen for this study. A strong consideration here was that the simplicity of the Monte Carlo RT concept should translate to reduced development time. Also, reversed Monte Carlo methods allow all computational effort to be concentrated on calculating radiances for the desired line of sight, and the nature of Monte Carlo algorithms makes parallel computing trivial.

Among the available backward Monte Carlo RT models, several do not allow a thermal source, or do not consider polarization fully (i.e., allowing a nondiagonal extinction matrix) (e.g., [5]), and some consider neither (e.g., [6] and [7]).

A useful reference for model development in this study, is the backward–forward Monte Carlo (BFMC) model described by [5]. In BFMC, photon paths are traced backward from the sensor, with scattering angles and path lengths randomly chosen from probability density functions (pdfs) determined by the scattering phase function, and a scalar extinction coefficient, respectively. The phase matrices for every scattering event and scalar extinction are then sequentially applied to the source Stokes vector to give the Stokes vector contribution for each photon. As presented in [5], the model is only applicable to cases where the extinction matrix is diagonal—that is, where there is macroscopically isotropic and mirror-symmetric scattering media. This prompted Roberti and Kummerow [8] to abandon the BFMC method and choose a modified forward Monte Carlo model. However, in [8] only a 1-D plane-parallel version of the modified forward Monte Carlo method was implemented.

In the study presented here, we demonstrate that it is possible to use a reversed Monte Carlo method for general polarized radiative transfer, and that the attractive features of Liu's backward–forward model can be retained by utilizing importance sampling, a well-known technique in Monte Carlo integration. Importance sampling allows independent variables, in this case scattering angles and path lengths, to be sampled from any distribution as long as each contribution to the final integral is properly weighted.

A radiative transfer program that includes scattering can share several elements with a program designed for clear sky radiative transfer. These shared components include clear sky radiative transfer, management of gaseous absorption coefficients, the representation of atmospheric fields, and propagation path calculation. To take advantage of this, the scattering algorithm described in this paper was added to the existing Atmospheric Radiative Transfer Simulator (ARTS) 1-1-x software package (http://www.sat.uni-bremen.de), which is modular and easily extendible. Development time was thus considerably reduced because many of the required components were already present. ARTS-1-1-x also includes a discrete-ordinates type scattering module, described in [9], the performance of which will eventually be compared with that of the Monte Carlo model presented here.

II. MODEL

The radiative transfer model solves the vector radiative transfer equation (VRTE)

$$\frac{d\mathbf{I}(\mathbf{n})}{ds} = -\mathbf{K}(\mathbf{n})\mathbf{I}(\mathbf{n}) + \mathbf{K_a}(\mathbf{n})I_b(T) + \int_{4\pi} \mathbf{Z}(\mathbf{n}, \mathbf{n}')\mathbf{I}(\mathbf{n}')d\mathbf{n}'$$
(1)

where $\mathbf{I}$ is the four-element column vector of radiances $\mathbf{I} = [I, Q, U, V]^T$ with units watts per square meter micron per meter per steradian ($W \cdot m^{-2}\mu m^{-1}sr^{-1}$). This will be referred to as the Stokes vector, although normally the Stokes vector is expressed in units of intensity. s is distance along direction $\mathbf{n}$, and I_b is the Planck radiance. $\mathbf{K}(\mathbf{n})$, $\mathbf{K_a}(\mathbf{n})$, and $\mathbf{Z}(\mathbf{n}, \mathbf{n}')$ are the bulk extinction matrix, absorption coefficient vector, and phase matrix of the medium, respectively. For brevity these have been expressed as bulk optical properties, where individual single-scattering properties have been multiplied by particle number density and averaged over all orientations and particle types. The argument $\mathbf{n}$ has been retained to signify that in general these properties depend on the direction of propagation.

To apply Monte Carlo integration to the problem, the VRTE needs to be expressed in integral form (e.g., [10])

$$\mathbf{I}(\mathbf{n}, \mathbf{s_0}) = \mathbf{O}(\mathbf{u_0}, \mathbf{s_0})\mathbf{I}(\mathbf{n}, \mathbf{u_0}) + \int_{\mathbf{u_0}}^{\mathbf{s_0}} \mathbf{O}(\mathbf{s}', \mathbf{s_0})$$

$$\times \left(\mathbf{K_a}(\mathbf{n})I_b(T) + \int_{4\pi} \mathbf{Z}(\mathbf{n}, \mathbf{n}')\mathbf{I}(\mathbf{n}')d\mathbf{n}'\right) ds' \quad (2)$$

where $\mathbf{O}(\mathbf{s}', \mathbf{s})$ is the evolution operator defined by [11]. $\mathbf{u_0}$ is the point where the line of sight intersects the far boundary of the scattering domain, and $\mathbf{s_0}$ is the exit point where the outgoing Stokes vector is calculated. In general, there is no closed-form

expression for $\mathbf{O}(\mathbf{s}', \mathbf{s})$. However, in cases where the extinction matrix is constant along a propagation path

$$\mathbf{O}(\mathbf{s}', \mathbf{s}) = \exp(-\mathbf{K}\Delta s).$$
(3)

In ARTS, a propagation path consists of a set of coordinates indicating where the path intersects with grid surfaces. If the extinction matrix in the path segment between two such points is considered constant, $\mathbf{K} = (\mathbf{K_j} + \mathbf{K_{j+1}})/2$, the evolution operator between two arbitrary points $\mathbf{s_0}$ and $\mathbf{s_N}$ is

$$\mathbf{O}(\mathbf{s_0}, \mathbf{s_N}) = \mathbf{O}(\mathbf{s_{N-1}}, \mathbf{s_N})\mathbf{O}(\mathbf{s_{N-2}}, \mathbf{s_{N-1}}) \ldots$$
$$\mathbf{O}(\mathbf{s_1}, \mathbf{s_2})\mathbf{O}(\mathbf{s_0}, \mathbf{s_1}) \quad (4)$$

where $\mathbf{O}(\mathbf{s_i}, \mathbf{s_{i+1}})$ is given by (3).

The numerical task is then to perform Monte Carlo integration on the integral on the right-hand side of (2). The aim in importance sampling is to choose pdfs for the independent variables that are as close as possible to being proportional to the integrand [12]. This concentrates computational effort on regions where the integrand is most significant and also reduces the variance in the contributions of each photon, thus reducing the number of photons and hence CPU time required to give a prescribed accuracy. (2) suggests that the pdf for sampling path length, where path length is the distance traced backward from the sensor, $\Delta s = |\mathbf{s} - \mathbf{s}'|$, should be proportional in some way to the evolution operator $\mathbf{O}(\mathbf{s}', \mathbf{s})$. Likewise, new incident directions $(\theta_{inc}, \phi_{inc})$ should be sampled from a pdf proportional to $\mathbf{Z}(\theta_{scat}, \phi_{scat}, \theta_{inc}, \phi_{inc})$. Since pdfs are scalar functions, and that we consider the first element of the Stokes vector most important, we choose pdfs that are proportional to the $(1,1)$ element of $\mathbf{O}(\mathbf{s}', \mathbf{s})$ and $\mathbf{Z}(\theta_{scat}, \phi_{scat}, \theta_{inc}, \phi_{inc})$.

A. Algorithm

The model algorithm proceeds as follows.

Step 1): Begin at the cloud box exit point with a new photon. Sample a path length, Δs along the first line of sight using the pdf

$$g_0(\Delta s) = \frac{\tilde{k}\tilde{O_{11}}(\Delta s)}{1 - O_{11}(\mathbf{u_0}, \mathbf{s_0})}$$
(5)

where $\tilde{O}_{11}(\Delta s)$ is the piecewise exponential function that includes $O_{11}(\mathbf{s}', \mathbf{s})$ values at points where the line of sight intersects with grid surfaces. Between two such adjacent intersections A and B the function $\tilde{O_{11}}(\Delta s)$ is given by

$$\tilde{O_{11}}(\Delta s) = O_{11}(\Delta s_A) \exp\left(-\tilde{k}(\Delta s - \Delta s_A)\right) \quad (6)$$

$$\tilde{k} = \frac{1}{(\Delta s_B - \Delta s_A)} \ln\left(\frac{O_{11}^A}{O_{11}^B}\right) \quad (7)$$

which, for cases where the extinction matrix is diagonal, is equal to $K_{11} = (K_{11}^A + K_{11}^B)/2$. The denominator in (5) ensures an emission or scattering event for each photon in the initial line of sight. Equation (5) is sampled by taking a random number (from the uniform distribution [0,1]) r and solving

$$\frac{1 - \tilde{O_{11}}(\Delta s)}{1 - O_{11}(\mathbf{u_0}, \mathbf{s_0})} = r$$
(8)

for Δs.

Step 2): Another random number r is drawn to choose between emission and scattering. We first define an albedo-like quantity

$$\tilde{\omega} = 1 - \frac{K_{a1}(\mathbf{n_0}, \mathbf{s_1})}{K_{11}(\mathbf{n_0}, \mathbf{s_1})}. \tag{9}$$

Note: We cannot use the actual single-scattering albedo as this depends on the polarization state of the incident radiation. If $r > \tilde{\omega}$, then the event is considered to be emission, the reversed ray tracing is terminated, and the Stokes vector contribution of the ith photon is

$$\mathbf{I^i}(\mathbf{n}, \mathbf{s_0}) = \frac{\mathbf{O}(\mathbf{s_1}, \mathbf{s_0})\mathbf{K_a}(\mathbf{n_0}, \mathbf{s_1})I_b(T, \mathbf{s_i})}{g_0(\Delta s)(1 - \tilde{\omega})} \tag{10}$$

where the index i signifies photon number. Return to Step 1).

Otherwise, if $r \leq \tilde{\omega}$ we have a scattering event.

Step 3): At the scattering point sample a new incident direction $(\theta_{inc}, \phi_{inc})$ according to

$$g(\theta_{inc}, \phi_{inc}) = \frac{Z_{11}(\theta_{scat}, \phi_{scat}, \theta_{inc}, \phi_{inc})\sin(\theta_{inc})}{K_{11}(\theta_{scat}, \phi_{scat}) - K_{a1}(\theta_{scat}, \phi_{scat})} \tag{11}$$

which is sampled by the rejection method as described in [12].

Calculate the matrix

$$\mathbf{Q_k} = \mathbf{Q_{k-1}}\mathbf{q_k} \tag{12}$$

where

$$\mathbf{q_k} = \frac{\sin(\theta_{inc})_k \mathbf{O}(\mathbf{s_k}, \mathbf{s_{k-1}})\mathbf{Z}(\mathbf{n_{k-1}}, \mathbf{n_k})}{g(\Delta s)g(\theta_{inc}, \phi_{inc})\tilde{\omega}} \tag{13}$$

and $\mathbf{Q_0} = \mathbb{1}$. The index k represents the scattering order.

Step 4): Choose a path length along the new direction according to

$$g(\Delta s) = \tilde{k}\tilde{O_{11}}(\Delta s). \tag{14}$$

This is sampled by taking a random number and solving

$$\tilde{O_{11}}(\Delta s) = r \tag{15}$$

for Δs. If $r < O_{11}(\mathbf{u_k}, \mathbf{s_k})$, where $\mathbf{u}_k$ is the boundary of the scattering domain in the current line of sight, the photon leaves the scattering domain, and the contribution for photon i is

$$\mathbf{I^i}(\mathbf{n}, \mathbf{s_0}) = \frac{\mathbf{Q_k}\mathbf{O}(\mathbf{u_k}, \mathbf{s_k})\mathbf{I}(\mathbf{n_k}, \mathbf{u_k})}{O_{11}(\mathbf{u_k}, \mathbf{s_k})} \tag{16}$$

where $\mathbf{I}(\mathbf{n_k}, \mathbf{u_k})$ is the incoming radiance at $\mathbf{u}_k$. This is calculated with the standard ARTS clear-sky routine. Return to Step 1).

Otherwise, if the sampled path length keeps the path within the scattering domain. . .

Step 5): As in Step 2), calculate $\tilde{\omega}$ at the new point $\mathbf{s_{k+1}}$ and draw a uniform random deviate r.

If $r > \tilde{\omega}$, then we have the following: the event is considered to be emission; the reversed ray tracing is terminated; the Stokes vector contribution is

$$\mathbf{I^i}(\mathbf{n}, \mathbf{s_0}) = \frac{\mathbf{Q_k}\mathbf{O}(\mathbf{s_{k+1}}, \mathbf{s_k})\mathbf{K_a}(\mathbf{n_k}, \mathbf{s_{k+1}})I_b(T, \mathbf{s_{k+1}})}{g(\Delta s)(1 - \tilde{\omega})} \tag{17}$$

and we return to Step 1).

Otherwise, if $r \leq \tilde{\omega}$ we have a scattering event and we return to Step 3).

Step 6): Once the prescribed number N of photon contributions $\mathbf{I^i}(\mathbf{n}, \mathbf{s_0})$ has been calculated, the cloud box exit Stokes vector is given by

$$\mathbf{I}(\mathbf{n}, \mathbf{s_0}) = \mathbf{O}(\mathbf{u_0}, \mathbf{s_0})\mathbf{I}(\mathbf{n}, \mathbf{u_0}) + \langle \mathbf{I^i}(\mathbf{n}, \mathbf{s_0}) \rangle \tag{18}$$

with an estimated error for each Stokes index j of

$$\delta I_j = \sqrt{\frac{\langle I_j^2 \rangle - \langle I_j \rangle^2}{N}}. \tag{19}$$

When simulating an MLS measurement, an extra clear sky RT calculation is performed from the cloud box exit to the sensor, with the Monte Carlo result from (18) taken as the radiative background.

B. Software Implementation

The above algorithm is contained within a module that has been added to the ARTS 1.1.x software package, which is being developed at several European Institutes. The software is written in C++ and is available under the Gnu General Public License. Some brief notes follow regarding details of the software implementation of the algorithm described above.

Atmospheric Grids: In ARTS, the atmosphere is gridded by latitude, longitude, and pressure coordinates. Because radiative transfer calculations with scattering are generally much more expensive than clear sky radiative transfer, scattering calculations are confined to a subdomain of the modeled atmosphere called the *cloud box*.

Scattering Properties: In this study, we consider spheroidal and cylindrical ice particles, with both completely random orientation or horizontally alignment with random azimuthal orientation. The single-scattering properties for these particles is obtained software derived from the random [13] and fixed [14] T-matrix codes of Mishchenko. Because of the computational expense of the T-matrix calculations, single-scattering properties are precalculated, imported in XML format, and interpolated as required. The complex refractive index of ice is obtained from the tabulated data of Warren [15].

Random Number Generation: Random numbers for path length and direction sampling are generated using the MT19937 generator of Matsumoto and Nishimura [16] as implemented in the GNU Scientific Library (http://www.gnu.org/software/gsl/).

Parallelization: The nature of the Monte Carlo algorithm makes utilization of multiple processors for single simulations trivial. The most straightforward method is to divide the desired number of photons among available processors and combine the results.

III. EXAMPLE RESULTS

Some example model output is shown in Fig. 2. The example atmospheric scenario was constructed by taking a 1-D profile of ice water content (IWC), temperature, and gas species mixing ratios from an MLS simulated data swath that has been used for Earth Observing System Microwave Limb Sounder (EOS-MLS) retrieval algorithm development. The 1-D IWC
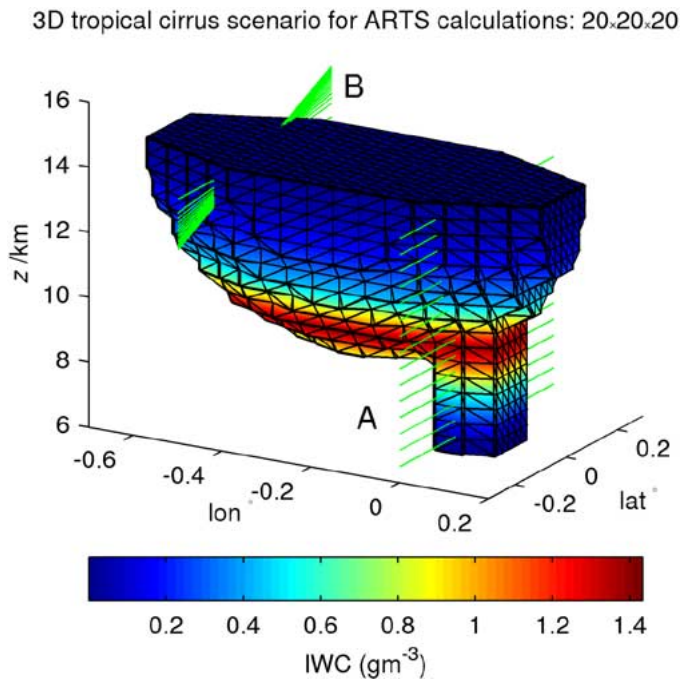
Fig. 1. Three-dimensional cloud scenario for example results.

profile was then superimposed on 3-D cloud shape resembling a tropical cumulonimbus anvil. Fig. 1 illustrates the cloud scenario, and also shows the lines of sight used in the radiative transfer simulations. The correlation of McFarquhar and Heymsfield [17] was used to obtain particle size distributions corresponding to IWC and temperature. This distribution was divided into 40 size bins for the calculation of single-scattering properties. Results are shown for three particle types: spheres, prolate spheroids (aspect ratio = 0.5), and oblate cylinders (aspect ratio = 2). Particle sizes are binned on an equal volume basis to conserve IWC. The blue curves in Fig. 2 are for horizontally aligned prolate spheroids; the particle rotation axes have a zenith angle of 90° and have a random azimuthal orientation angle. The cyan curves are for the same particles but with completely random orientation. The red curves are for horizontally aligned oblate cylinders, where the axes of rotation are parallel with the local zenith. These different microphysical scenarios were selected to demonstrate the model's capability rather than to accurately reflect an actual cirrus cloud.

The frequency considered here, 200.5 GHz, is in the upper side-band of band 2 on Radiometer 2 of the EOS-MLS instrument. In these tests two sets of viewing directions, labeled A and B in Fig. 1, are considered. Both sets consider the same tangent heights, $6.5 \text{ km} \leq z_{tan} \leq 13.5 \text{ km}$, but have a different scheme for placing the sensor relative to the cloud. In set A the sensor is positioned so that the tangent point lies within the cloud, at (0N,0E). In set B each line of sight passes through (0N,−0.5E, 13.5 km), so that the tangent point is either in or behind the cloud when viewed from the sensor.

In these simulations the cloud-box was determined from the extent of the cloud shown in Fig. 1, and was discretized on a $20 \times 20 \times 20$ grid. This grid was then merged with a $100 \times 100 \times 100$ grid spanning the modeled atmosphere to give a combined $120 \times 120 \times 120$ grid. The modeled atmosphere must be large
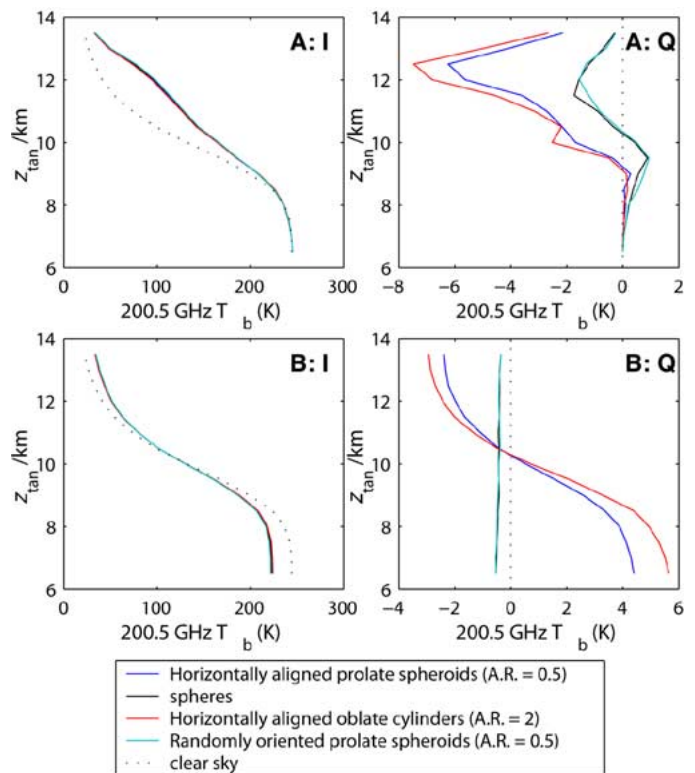

Fig. 2. Simulated single sideband EOSMLS radiances, I, and polarization differences, $Q = I_v - I_h$, for 200.5 GHz. The cloud scenario for these simulations is shown in Fig. 1.

enough so that no propagation path can enter the cloud box from a point on any side boundary of the modeled atmosphere.

For each simulation 4×10^5 photons were used. Each simulation was run on a single 2.8-GHz CPU.

A. Results

Fig. 2 shows values for the total radiance, $I = I_v + I_h$, and polarization difference, $Q = I_v - I_h$, for the simulations described above. Both quantities are expressed as Rayleigh–Jean brightness temperature. The other Stokes elements U and V are not shown as their magnitude is insignificant in comparison with I and Q. The top row of plots are for viewing direction set A, and the bottom row is for set B.

The first column of plots in Fig. 2 indicates that the choice of particle type and orientation scheme had little effect on the total radiance. However, particle type and orientation did have a significant impact on the polarization difference. Although randomly oriented prolate spheroids behaved almost exactly like spherical particles (of the same volume), the horizontally aligned prolate spheroids and oblate cylinders gave significant partial horizontal or vertical polarization—depending on the viewing direction. For simulation set A, the horizontally aligned particles gave partial horizontal polarization for tangent heights above 9 km. For simulation set B, the horizontally aligned particles gave partial horizontal polarization for tangent heights above 10.5 km but partial vertical polarization for tangent heights below 10.5 km. The sign of the polarization signal is determined by the magnitude of two opposing mechanisms: dichroism, as manifest by a nondiagonal extinction matrix,
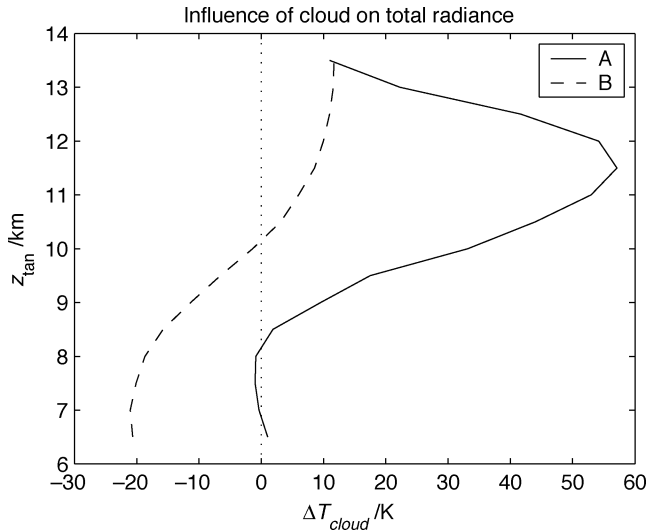
Fig. 3.   Influence of the cloudy scenario in Fig. 1 (with horizontally aligned prolate spheroids) on the total radiance, $\Delta T_{cloud} = I_{cloudy} - I_{clear}$, for viewing direction sets A and B.

K; and the effect of radiation being scattered into the line of sight. In the cases presented here, the horizontally aligned nonspherical particles have a negative K_{21}, which has the effect of vertically polarizing radiation. The magnitude of this effect on the measured radiance depends on the source radiance. The contribution to the polarization signal of radiation scattered into the line of sight depends on both the spatial distribution of incoming radiance, and the shape and orientation of scattering particles, which, in the case of horizontally aligned particles, contributes to horizontal polarization. The mechanisms above combine to give the different Q profiles for cases A and B. In both cases for high tangent heights the radiative background is cold so that the dichroism effect is small in comparison with the scattering integral contribution. This yields the partial horizontal polarization (negative Q) at high tangent heights; Q is more negative in case A because of the greater path length within the cloud and for a given tangent height the path in case A traverses a warmer part of the cloud, thus increasing the scattering integral contribution. The warmer source radiance at low tangent heights increases the dichroism effect—giving positive Q in case B. Case A does not exhibit positive Q at low tangent heights because of the dominance of gaseous emission and absorption between the cloud and the sensor.

Cases A and B also produce significantly different radiance profiles, as demonstrated in the first column of Fig. 2. This difference is clarified by Fig. 3, where the difference between cloudy sky and clear sky radiance $\Delta T_{cloud} = I_{cloudy} - I_{clear}$ is plotted for cases A and B with the cloud composed of horizontally aligned prolate spheroids. In both cases, there is a positive ΔT_{cloud} for high tangent heights due to the scattering of warm radiances into the line of sight; the effect is greater in case A due to the increased length and decreased altitude of the in-cloud optical path. At low tangent heights in case B, the cloud has a negative impact on the simulated radiance; this is not observed in case A due to the placement of the tangent point within the cloud, and the dominance of gaseous emission and absorption between the cloud and the sensor.
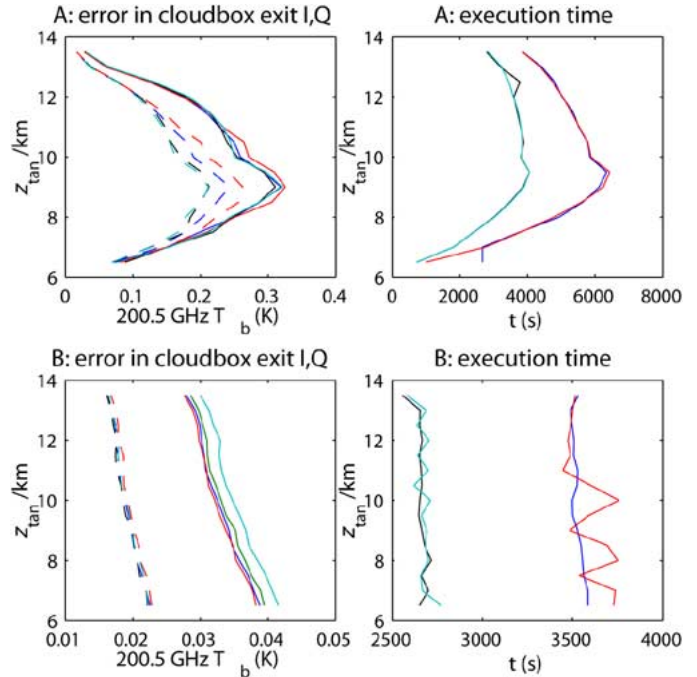

Fig. 4.   Estimated error in cloud-box exit radiance (solid) and polarization difference (dashed) for the simulations presented above. Line colors are as in Fig. 2. The right column shows the execution time for each simulation.

B. Performance

Fig. 4 shows the estimated error in the first two elements of the cloud-box exit Stokes vector for all of the example simulations. These were obtained from the Monte Carlo algorithm by (19). To get an estimate of the error of the simulated measured radiance, these values must be multiplied by the clear sky transmittance between the cloud-box and the sensor. These plots show that the estimated error in cloud-box exit Stokes vector is strongly dependent on the optical thickness in the line of sight, and relatively independent of particle type and orientation.

Although the absolute error in polarization difference is generally lower than that for total radiance, the relative error is much higher. This is apparent in the top right panel of Fig. 2, where some noise is evident at intermediate tangent heights, where cloud-box exit Stokes vector error is largest. Therefore in some cases, where accurate Q determination is desired, it may be necessary to increase the number of photons used in the simulation.

The second column of plots in Fig. 4 show the time taken for each simulation. These values obviously depend on a range of factors to do with the computing environment and compilation options. However, the plots do demonstrate that CPU time, like cloud-box exit Stokes vector error, is strongly dependent on ice water path and the IWC of the scattering domain. Also, the calculations involving horizontally aligned particles were considerably more expensive than those for spheres or randomly oriented particles. This reflects the additional cost of nondiagonal extinction matrices and the extra angular dependencies of optical properties for horizontally aligned particles.

Memory use for each of the example simulations was 300 MB or less.

IV. DISCUSSION AND FUTURE WORK

A reversed Monte Carlo algorithm has been presented for 3-D polarized transfer in millimeters and submillimeter remote sensing applications. Although 3-D polarized radiative transfer calculations are computationally demanding, the example limb sounding simulations shown in this paper demonstrate that the software implementation of the algorithm provides acceptable accuracy, and execution times that are practical for use in research. Like the rest of the ARTS package, this software is freely available under the Gnu General Public License and can be downloaded from http://www.sat.uni-bremen.de.

Although the example simulations presented here are only intended to illustrate the capabilities of the radiative transfer model, the results suggest that it is important to consider more than one spatial dimension and also polarization when simulating microwave limb sounding measurements. The results showed two significant effects that cannot be reproduced by a 1-D radiative transfer model: the effect of inhomogeneity of cloud properties in the latitude/longitude coordinates, and the location of the cloud field relative to the sensor. The results also showed significant polarization effects due to oriented nonspherical particles. If one were to attempt a 1-D representation of the cloud field shown in Fig. 1, with the assumption of equivalent spheres, then the variation in Stokes vector profiles shown in Fig. 2 would be lost.

It is planned to use the model presented here to study the influence of cirrus microphysics and macroscopic structure on EOS-MLS radiances. It is hoped that this work will increase the amount and quality of cloud information retrieved by EOS-MLS. Although the scattering model was developed with microwave limb sounding in mind, it is also directly applicable to other viewing geometries.

ACKNOWLEDGMENT

REFERENCES

[1] S. T. Bond, "The potential effect of cirrus on Microwave Limb Sounder retrievals," Ph.D. dissertation, Univ. Edinburgh, Edinburgh, U.K., 1996.

[2] D. L. Wu and J. H. Jiang, "EOS MLS algorithm theoretical basis for cloud measurements," Jet Propulsion Lab., Pasadena, CA, Tech. Rep., 2002.

[3] K. F. Evans, "The spherical harmonics discrete ordinate method for three-dimensional atmospheric radiative transfer," *J. Atmos. Sci.*, vol. 55, pp. 429–446, 1998.

[4] A. Macke, D. L. Mitchell, and L. V. Bremen, "Monte carlo radiative transfer calculations for inhomogeneous mixed phase clouds," *Phys. Chem. Earth (B)*, vol. 24, no. 3, pp. 237–241, 1999.

[5] Q. Liu, C. Simmer, and E. Ruprecht, "Three-dimensional radiative transfer effects of clouds in the microwave spectral range," *J. Geophys. Res.*, vol. 101, no. D2, pp. 4289–4298, 1996.

[6] L. Oikarinen, E. Sihvola, and E. Kyrola, "Multiple scattering radiance in limb-viewing geometry," *J. Geophys. Res.*, vol. 104, no. D24, pp. 31 261–31 274, 1999.

[7] K. Ishimoto and H. Masuda, "A Monte Carlo approach for the calculation of polarized light: Application to an incident narrow beam," *J. Quant. Spectrosc. Radiat. Transf.*, vol. 72, no. 4, pp. 462–483, 2002.

[8] L. Roberti and C. Kummerow, "Monte carlo calculations of polarized microwave radiation emerging from cloud structures," *J. Geophys. Res.*, vol. 104, no. D2, pp. 2093–2104, 1999.

[9] C. Emde, S. A. Buehler, C. Davis, P. Eriksson, T. R. Sreerekha, and C. Teichmann, "A polarized discrete ordinate scattering model for simulations of limb and nadir long-wave measurements in 1-D/3-D spherical atmospheres," *J. Geophys. Res.*, vol. 109, no. D24, D24207, 2004. DOI: 10.1029/2004JD005140.

[10] H. Hochstadt, *Differential Equations: A Modern Approach.* New York: Holt, Rinehart, and Winston, 1964.

[11] E. L. Degl'Innocenti and M. L. Degl'Innocenti, "On the solution of the radiative-transfer equations for polarized radiation," *Solar Phys.*, vol. 97, no. 2, pp. 239–250, 1985.

[12] J. Liu, *Monte Carlo Strategies in Scientific Computing.* Berlin, Germany: Springer-Verlag, 2001.

[13] M. Mishchenko and L. Travis, "Capabilities and limitations of a current FORTRAN implementation of the T-matrix method for randomly oriented, rotationally symmetric scatterers," *J. Quant. Spectrosc. Radiat. Transf.*, vol. 60, no. 3, pp. 309–324, 1998.

[14] M. Mishchenko, "Calculation of the amplitude matrix for a nonspherical particle in a fixed orientation," *Appl. Opt.*, vol. 39, no. 6, pp. 1026–1031, 2000.

[15] S. Warren, "Optical constants of ice from the ultraviolet to the microwave," *Appl. Opt.*, vol. 23, no. 8, pp. 1206–1225, 1984.

[16] M. Matsumoto and T. Nishimura, "Mersenne twister: A 623-dimensionally equidistributed uniform pseudorandom number generator," *ACM Trans. Modeling Comput. Simul.*, vol. 8, pp. 3–30, 1998.

[17] G. McFarquhar and A. Heymsfield, "Parametrization of tropical ice crystal size distributions and implications for radiative transfer: Results from CEPEX," *J. Atmos. Sci.*, vol. 54, pp. 2187–2200, 1997.

Cory Davis received the B.Sc. (Hons,1) and Ph.D. degrees in physics from the University of Otago, Dunedin, New Zealand, in 1996 and 2001, respectively.

He is currently a Postdoctoral Research Fellow with the Institute for Atmospheric and Environmental Science at the University of Edinburgh, Edinburgh, U.K. He is a member of the Microwave Limb Sounding team at this institute and is funded under the NERC Clouds, Water Vapor, and Climate (CWVC) thematic program. His primarily research interest is the influence of Cirrus on EOS-MLS trace gas and cloud property retrievals.

Claudia Emde received the diploma degree in physics from the University of Bremen, Bremen, Germany, in 2001, where she is currently pursuing the Ph.D. degree at the Institute of Environmental Physics.

She is a member of the Satellite Microwave Atmospheric Sounding Group and is funded by the German Federal Ministry of Education and Research (BMBF), within the DLR project SMILES, grant 50 EE 9815. Her research interest is radiative transfer modeling to study the impact of cirrus clouds on microwave radiation in the atmosphere.

Robert Harwood graduated in mathematics and received the Ph.D. degree in meteorology from Imperial College London, London, U.K., in 1964 and 1969, respectively.

He is currently a Professor of atmospheric science in the School of Geosciences at Edinburgh University, Edinburgh, U.K. He spent seven years as a Senior Research Officer at the (then) Department of Atmospheric Physics at Oxford University. There, he developed an interest in modeling and remote sensing of the dynamics and composition of the atmosphere, with over 60 publications in refereed journals. He is a NASA-accredited Co-Investigator on the Microwave Limb Sounder on the Aura Satellite, and a Principal Investigator for the U.K. section of the science team.